
In situ carbon and oxygen isotopes measurements in carbonates by fiber coupled laser diode-induced calcination: A step towards field isotopic characterization

Thomazo Christophe ^{1,2,*}, Sansjofre Pierre ³, Musset Olivier ⁴, Cocquerez Theophile ¹, Lalonde Stefan ⁵

¹ Biogéosciences, CNRS UMR 6282, Université Bourgogne Franche-Comté, France

² Institut Universitaire de France, France

³ Muséum National d'Histoire Naturelle, Sorbonne Université, CNRS UMR 7590, IMPMC, 75005 Paris, France

⁴ Laboratoire Interdisciplinaire Carnot de Bourgogne, CNRS UMR 6303, Université de Bourgogne Franche-Comté, France

⁵ Laboratoire Géosciences Océan, Institut Universitaire Européen de la Mer, CNRS UMR 6538, France

* Corresponding author : Christophe Thomazo, email address : christophe.thomazo@u-bourgogne.fr

Abstract :

Natural stable isotopes ratios ($\delta^{13}\text{C}_{\text{carb}}$ and $\delta^{18}\text{O}_{\text{carb}}$) of carbonates archived in the geological record are routinely used to reconstruct local and global paleo temperatures and the secular evolution of the biogeochemical carbon cycle. The state-of-the-art technique, employed since the mid 20th century, to measure these isotopic ratios starts with field sampling followed by several steps of physical and chemical laboratory preparation including: (i) microdrilling and/or sawing and crushing, (ii) CO₂ release by wet acid digestion, (iii) gas equilibration, purification and transfer, before (iv) gas phase IRMS measurements. While these steps are time and resource consuming, they provide accurate measurements of $\delta^{13}\text{C}_{\text{carb}}$, $\delta^{18}\text{O}_{\text{carb}}$ and carbonate contents. This study presents a new protocol involving a compact and modernized laser calcination system that decreases drastically the analyses time by reducing the number of preparations steps together with offering the possibility of performing spatially resolved analysis at the mm scale. This new method is based on the use of a fiber coupled laser diode device emitting 30 W in the near infrared at 880 nm. The energy provided by the laser source induces the decomposition of calcium carbonate into lime and carbon dioxide. In this work, the CO₂ was collected in sample tubes under a controlled atmosphere for offline analysis, however additional developments should permit online analysis in the near future.

We analyzed 9 different types of carbonate minerals encompassing a range of isotopic compositions VPDB between +3.3 and -18.2‰ and between -1.7 and -14.6‰ for $\delta^{13}\text{C}_{\text{carb}}$ and $\delta^{18}\text{O}_{\text{carb}}$, respectively. A comparison of isotopic results was performed for carbonate zones analyzed both by classic methods (micro-drilling followed by acid digestion) and laser calcination. This isotopic cross-calibration exercise shows a direct positive co-variation between both methods with a correlation coefficient of 0.99 and a regression slope of 1 within uncertainties for the $\delta^{13}\text{C}_{\text{carb}}$ values. The $\delta^{18}\text{O}_{\text{carb}}$ values also compared well with a correlation coefficient of 0.96, suggesting a constant gas-solid phase isotopic equilibrium between carbon dioxide and lime. The reproducibility of our laser calcination method performed on replicate analyses of dolomite, siderite and malachite shows a 1 σ standard deviation of

0.31 and 0.77 for $\delta^{13}\text{C}_{\text{carb}}$ and $\delta^{18}\text{O}_{\text{carb}}$, respectively. These reproducibilities are within the observed isotopic natural inhomogeneity of samples (up to 1.3 and 0.57‰ for the $\delta^{13}\text{C}_{\text{carb}}$ and $\delta^{18}\text{O}_{\text{carb}}$, respectively) as assessed by microdrilling and acid digestion.

Based on the suit of samples analyzed in this study, we demonstrate that (i) fiber coupled laser diode calcination enables accurate and reproducible C and O isotopic characterization of natural carbonates, (ii) physical effects during calcination do not introduce any isotopic fractionation for C and is accompanied by a constant isotopic offset for O over a range of isotopic compositions and mineral matrices. These findings pave the way for a new range of possibilities for carbonate $\delta^{13}\text{C}$ and $\delta^{18}\text{O}$ measurements directly in the field using rapid, portable, and easy to manipulate laser preparation devices paired with CRDS/IRIS optical-mass spectrometers.

Keywords : Carbon isotopes, oxygen isotopes, carbonates, laser, carbon cycle

1. Introduction

Carbonates are among the most widely distributed minerals in the Earth's crust and more than 3.5 billion years of Earth's history are chronicled in these rocks. Carbonates play a major role in the global carbon cycle and in particular the long-term sequestration of atmospheric CO₂ in sediments via silicate weathering followed by carbonate precipitation (Berner et al., 1983). The latter played a critical role in differentiating Earth's atmosphere from that of Mars, Venus or Mercury, and is ultimately responsible for ensuring the habitability of our planet by keeping CO₂ in the trace gas concentration range (Walker et al., 1981).

Understanding how carbonates are produced, from the formation of thin sedimentary layers to the evolution of regional carbonate platforms, is a major scientific challenge that has largely benefited from the study of their stable isotope compositions. Up to now these measurements have been largely performed using wet chemical preparation of the samples before Isotope Ratio Mass Spectrometer (IRMS) analyses (McCrea, 1950) in a dedicated laboratory environment. In recent years however, the development of a new generation of compact gas phase IRMS instruments based on technologies such as Cavity Ring Down Spectroscopy (CRDS) or Isotope Ratio Infrared Spectrometry (IRIS) now permit the analysis of atmospheric CO₂ carbon and oxygen stable isotope ratios directly in the field (e.g. Garcia-Anton et al., 2014; Rizzo et al., 2014; Fisher et al., 2016). A major barrier to the use of these field-deployable instruments to measure the $\delta^{13}\text{C}$ and $\delta^{18}\text{O}$ of carbonates are the traditional sample preparation steps: (i) crushing or microdrilling (with an optimal final grain size lower than 140 μm), (ii) transfer of sample powder into vials, (iii) evacuation of residual air by flushing with CO₂-free gas, and finally (iii) sample digestion using several drops of orthophosphoric acid (H₃PO₄; McCrea, 1950). The reaction time is generally between 15min and 48h, depending on carbonate mineralogy, before isotopic measurements can be performed on the CO₂ evolved from the carbonate sample. While this entire process is long and time consuming, it provides accurate values of $\delta^{13}\text{C}_{\text{carb}}$, $\delta^{18}\text{O}_{\text{carb}}$ and carbonate content with typical internal reproducibility of isotope ratios better than 0.1‰.

In situ laser extraction techniques were first developed in the 1990's to offer a rapid, simple and high spatial resolution alternative to the conventional methods

describe above (Smalley et al., 1989; Smalley et al., 1992; Sharp, 1992; Sharp and Cerling, 1996; Cerling and Sharp, 1996; Spötl and Matthey, 2006; McDermott, 2005; Cosford et al., 2008; Hodge et al., 2008; Cosford et al., 2009; Cosford et al., 2010; Baker et al., 2011; Baldini et al., 2015). For example, Sharp and colleagues (Sharp, 1992; Sharp and Cerling, 1996; Cerling and Sharp, 1996) proposed a laser calcination technique using a 20W CO₂ laser (beam size >80µm) with a pulse generator. The CO₂ is produced by calcination, following equation (1):



In this earlier set up, evolved CO₂ is frozen in a cold trap at liquid nitrogen temperature, then transferred to an IRMS mass spectrometer. In Sharp and Cerling, (1996), results were provided for 6 different types of carbonate minerals: calcite, dolomite, magnesite, rhodochrosite, siderite, and smithsonite. They reported an average reproducibility of 0.3‰ for δ¹⁸O_{carb} and 0.1‰ for δ¹³C_{carb} (1σ).

While these laser techniques clearly simplify sample preparation and permit spatially resolved analysis, they still require cumbersome equipment, including a CO₂ laser (see supplementary information for size and weight characteristics), a liquid nitrogen tank or a temperature regulated GC system, and an IRMS mass spectrometer, which are all prohibitive to deployment outside of the laboratory.

The emergence of smaller, lighter and portable optical mass spectrometers based on CRDS or IRIS, together with modern miniaturized laser sources, pave the way to an entire new approach to carbon and oxygen isotopic measurements, including the possibility of in situ isotopic mass spectrometry performed in the field. We propose in this study a new technique and protocol for δ¹³C_{carb} and δ¹⁸O_{carb} analyses based on laser calcination using a portable fiber coupled laser diode device that could be easily paired to a CRDS/IRIS optical spectrometer.

2. Conceptual frame work of laser calcination physics

The reasoning of using a laser to trigger calcination reactions relies on local material-light interactions as a spatially resolved source of heat. The incident laser radiation is focused on a small area of the sample and the fraction of radiation not reflected or scattered can then be absorbed by the material. Most of the absorbed

energy is then released quickly in the form of heat in a very small volume, which leads to rapid and localized heating. This local heating allows the sample to reach spontaneous calcination temperature and release CO₂. Complex models resolved in space and time describing the laser calcination processes for rock cutting applications can be found in the literature for different laser wavelengths and power (Othman et al., 2019; Turchetta and Carrino., 2005; San-Roman-Alerigi et al., 2017; San-Roman-Alerigi et al., 2018).

This work does not present detailed numerical modelling because it is beyond the scope of this contribution. However, we consider in this study that the incident energy of the laser beam is the sum of the reflected, diffused, absorbed and transmitted end members. As the absorption coefficients of the materials are high in the visible or near infrared, it can be considered that all of the transmitted radiation is absorbed over a shallow depth. The absorbed energy E_{abs} can therefore be considered as the product of the emissivity ε of the material multiplied by the incident laser energy E_{laser} (equation 2). It follows that the energy can be express as the difference between incident power P_{laser} minus reflected power $P_{reflected}$ multiplied by the duration of exposure Δt

$$E_{abs} = \varepsilon \cdot E_{laser} = (P_{laser} - P_{reflected}) \cdot \Delta t \quad (2)$$

Considering that all of the energy absorbed is transformed into heat, this energy can be express as the sum of the energy of material heating (equation 3), enthalpy of calcination, and heat losses (e.g. thermal conduction or ejection of material or even radiation of the black body).

$$E_{abs} = E_{Heat} + E_{calcination} + E_{thermal losses} \quad (3)$$

Considering this energy balance, it is necessary to reach temperatures of around 900-950°C in order to trigger calcination reaction (Engler et al., 1989; Turchetta and Carrino, 2005). Moreover, the heating energy depends not only on the thermal and mechanical properties of the materials but also optical properties such as emissivity and absorption coefficient. Similarly, the enthalpy of calcination depends on the chemical structure (i.e. mineral lattice) and composition of the

sample (Othman et al., 2019). The balance between all these effects is complex, (but excludes in our case the melting of lime which occurs at ca. 2570°C according to Turchetta and Carrino (2005). The heat affected zone (i.e. HAZ) can also develop a cooler zone in the middle which results from the ejection of produced lime powder by CO₂. This can further complicate the energetic balance. To trigger calcination, it is therefore necessary to provide sufficient energy per unit of volume and time to reach the calcination temperature (100-200kJ / mol) and provide an energy equivalent to the enthalpy of calcination (50-100kJ / mol). The calcination thresholds and the production of CO₂ as a function of laser energy will therefore be very dependent on the material exposed.

In the following sections, the laser intensity at the focal point is also considered in addition to the laser energy or laser power (see supplementary information for detailed information on laser optical characteristics and a comparison of fiber coupled laser diode modules with CO₂ lasers). For this, the radius of the laser spot ω_0 is considered on the sample at the focal point of a lens of focal length f , for a laser source with a Gaussian spatial profile quality of beam M^2 , of wavelength λ and beam diameter at the entry of the lens W_{in} (equation 4):

$$\omega_0 = \frac{4 \cdot M^2 \cdot \lambda \cdot f}{\pi \cdot W_{in}} \quad (4)$$

The intensity I can then be written as the ratio between the incident power of the laser divided by the surface at the focal point (equation 5):

$$I = \frac{P_{laser}}{\pi \omega_0^2} \quad (5)$$

3. Material and methods

3.1 Sample descriptions

Nine different types of carbonate minerals archetypal of Earth's chemical and isotopic diversity have been selected for this study and are listed in Table 1. The samples (see supplementary information for pictures) have been chosen in order to reflect a large range in chemical composition, type of matrix, grain size and colour. Preliminary tests demonstrated that transparent varieties of carbonate, such as

Iceland spar, showed poor calcination characteristics due to their very low absorption coefficient in the near-IR range, and were discarded from the study.

	Sample	Description	Formula	Origin	ID number
1	Calcite 1	Speleothem	CaCO ₃	DMC	nr
2	Calcite 2	Ferroancalcite	CaCO ₃	DMC	nr
3	Dolomite 1	Micrite	CaMg(CO ₃) ₂	DMC	76-5
4	Dolomite 2	Saccharoid	CaMg(CO ₃) ₂	Saxony (DMC)	912
5	Siderite	Macrocrystal	FeCO ₃	DMC	nr
6	Malachite	Macrocrystal	Cu ₂ CO ₃ (OH) ₂	Siberia (DMC)	472
7	Rhodocrosite	Macrocrystal	MnCO ₃	Rothenberg Mine (DMC)	985
8	SDV	Dolomicrite	CaMg(CO ₃) ₂	Noonday Fm. (USA)	nr

Table 1: Carbonate mineral list and sample characteristics. Sample: name of the sample. Description: main lithological aspect. Formula: chemical formula of the considered carbonate. Origin: Dijon Museum Collection (DMC). Number: inventory number. Nr: Non-referenced material. SDV is a Neoproterozoic stromatolitic cap dolostone (Mg/Ca ratio of 0.52) deposited around 635 Ma in the aftermath of the Marinoan Snowball Earth.

3.2 Carbon and oxygen isotope analyses

All stable isotope analyses were performed at the Biogeosciences Laboratory, Université Bourgogne Franche-Comté, Dijon, France.

Samples were analysed twice using state of the art micro-drilling and wet chemistry preparation before IRMS analyses (McCrea, 1950) and using the laser calcination device described in detail below.

Samples were first micro-drilled several times (between 10 and 15) depending on the size of the samples in order to estimate spatial isotopic homogeneity. Then, 50 to 100 µg of each micro-drilled powders were loaded in glass vials and reacted with a 102% H₃PO₄ solution at 70°C for 20 minutes. Carbon and oxygen isotopic compositions were measured on a ThermoScientific™ Delta V Plus™ IRMS coupled with a Kiel VI carbonate preparation device. All isotope values are reported in the standard δ-notation (in ‰) relative to the international standard VPDB (Vienna Pee Dee Belemnite) using a δ¹³C value of +1.95‰, and a δ¹⁸O value of -2.20‰ for the international standard NBS19 (Coplen et al., 2006) analyzed in the same sessions. External reproducibility was assessed by replicate analyses of both NBS19 and in-house laboratory calcite and dolomite standards and is better than ±0.07‰ (2σ). Specific oxygen isotopes fractionation factor between H₃PO₄ and evolved CO₂ due to

cationic solid substitution (Rosenbaum and Sheppard, 1986; Böttcher, 1996) are not considered in this study.

Samples were then loaded in the laser device (see section 3.3), and the evolved CO₂ produced after laser calcination was collected in glass tubes and connected to the dual inlet sample port of the ThermoScientific™ Delta V Plus™ IRMS. Samples were then analysed against the Dijon Biogeosciences Laboratory in-house reference gas. A mass to charge ratios (m/z) scan of these samples was also performed following the isotopic analyses.

Before and after each “laser analytical session”, the in-house reference gas was verified for its calibration vs VPDB by analysing NBS19 international standards in “Kiel” mode.

3.3 Laser analytical system

The laser source is a laser diode with a maximum output power of 30 W and an emission wavelength around 880 nm (JOLD[®]) connected to an optical fiber 200 μm in diameter with a numerical aperture of 0.22. This laser module is manufactured in large series and generally used as an optical pumping source in solid state lasers; it is efficient at high optical / electrical efficiency (≥30%), inexpensive (<2k€), small (90x50x25 mm) and light (0.25 kg) and is available from many manufacturers. The laser source is mounted on two Peltier modules and a heat sink to control and regulate the temperature of the laser diode and to stabilize its operation in wavelength to around 880 nm at 28°C. The laser output power is controlled by an adjustable current power supply from 0 to 42 A which corresponds to a variable laser power at the optical fiber output from 0 to 25 W. The laser is integrated in a lab-made compact and portable “control box” which also includes switching power supply modules, allowing it to be fitted with either a mains power adapter or a battery (including a car battery) under a large input voltage range. It also includes a user interface and several electronic drivers based on an Arduino® Due single board computer and a color touch screen associated with a color video LCD screen that imaged the surface of the sample. Specific software has been developed to control all laser parameters (current and therefore laser power, temperature, duration of power rise and fall time, continuous or pulse operation, etc.) and accessories. A double security system with two different keys (general ON / OFF, and laser firing authorization) also makes it possible to secure the access to the laser, which is very

important given the high power of the laser (class IV laser). The optical fiber from the laser module and the electrical cable for controlling the accessory functions are then connected to an optical unit for shaping, focusing, targeting and viewing the sample. This unit includes an optical system for collimating and focusing the laser beam at the output of the optical fiber. It is composed of two achromats (50 and 100 mm from Thorlabs®) with a focal length of approximately 100 mm corresponding to a laser spot of 400 μm in diameter and a depth of field (assuming $\pm 10\%$ variations on the diameter) of approximately ± 1.0 mm. The optical unit is associated with two laser sighting diodes (@ 630 nm) crossing at the focal point of the power laser beam in the focal plane. The aim of this system is to allow precise targeting of the sample in complete safety. The optical unit is also mounted on a vertical translation system to adjust the focal plane on the surface of the sample which can have variable thickness. Under the optical unit is then mounted a 45° dichroic separator, which allows the near infrared to be transmitted and visible wavelengths reflected to a color video camera. This camera has a low-pass filter which protects it from laser light reflected or scattered by the sample in order to prevent damage.

The sample is introduced in a Foral® alloy chamber (Figure 1). It includes on top a large diameter BK7 optical window (50 mm, broadband AR coatings of both faces, Edmund®) and a side window to observe the laser material interaction or for example place other optical sensors (spectrometers, photodiodes).

The sample chamber has three ports. (i) the first port is used for evacuating the chamber using a primary vacuum pump or for injecting gas (ambient air, synthetic air, nitrogen, argon, etc.) into the chamber. It includes two solenoid valves to switch from one operating mode to the other. (ii) the second port is connected to a pressure probe (Pirani gauge with range from 1mbar to 1.4bar, Tyracont®). (iii) the third port is used to connect either a glass sample tube or a pump to drive the gas produced, for example, to an optical spectrometer of IRIS or CRDS type.

Inside the sample chamber are also arranged several sensors including a thermistor sensor (10k Ω NTC) for measuring the temperature under the sample, a second compact pressure probe (MPX4115, NXP®) and an atmospheric control module capable of measuring the concentration of CO₂ (in ppm), humidity and temperature (SCD30, Sensirion®). This module is designed to work around atmospheric pressure with a slow response time (one acquisition every two seconds, and reliable measurement obtained in one to a few minutes) and does not allow

measurement of the evolution of CO₂ in real time. However, it allows the quantity of CO₂ produced during laser irradiation to be quantified after allowing sufficient measurement time. The sample chamber sensors are controlled by a second Arduino® Due module which directly displays the measured data and their variations on a compact color screen. The sample chamber is fitted on a micrometric motorized XY movement platform mounted on an air cushion and controlled by a third Arduino® Due module.

Overall, the laser system, presented on the Figure 1, is compact and easily transportable, with a small and light fiber coupled laser diode paired with a compact and portable control box.

Journal Pre-proof

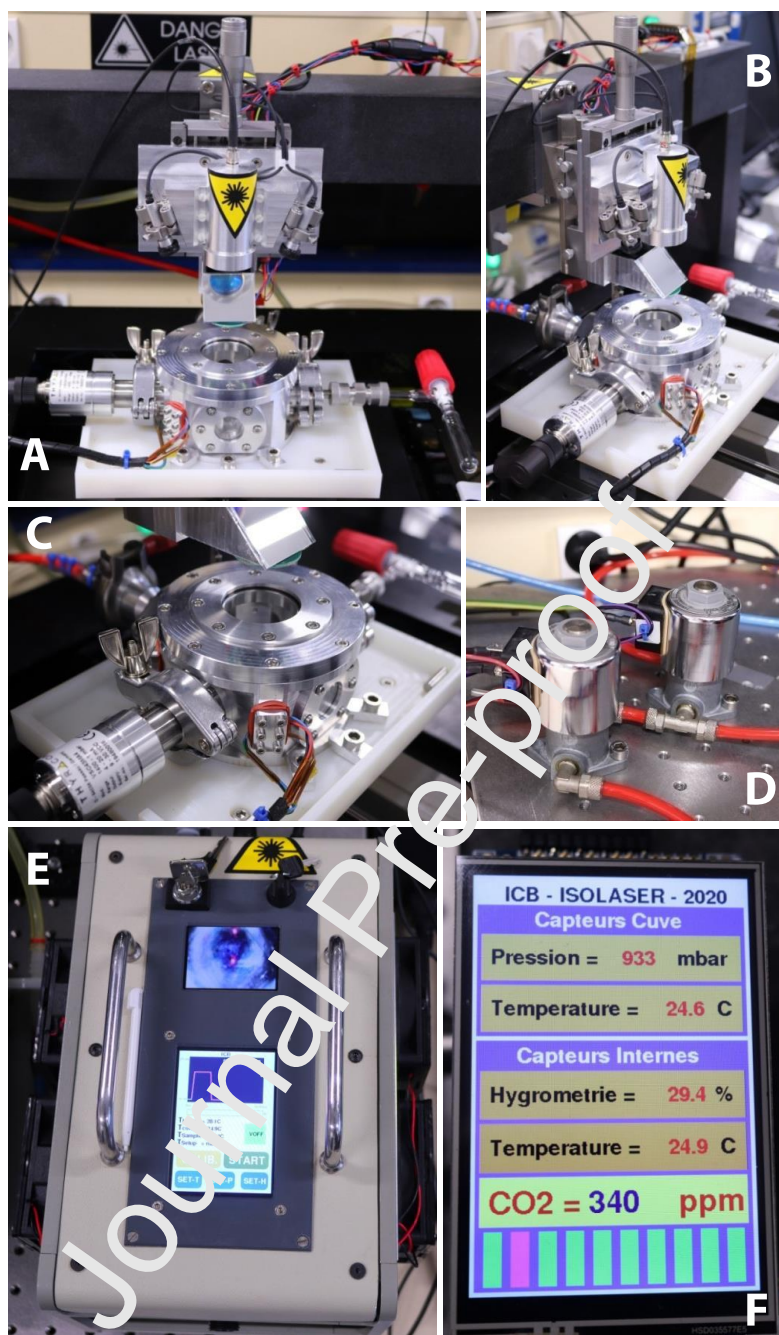


Figure 1: Photographs of the laser analytical system installed in the Laboratoire Interdisciplinaire CARNOT, Université de Bourgogne Franche-Comté, France. A and B front and side view of the laser analytical system; C close up view of the sample chamber with glass sample tube port on the right and pressure gage fitting on the left; D solenoid valves allowing to switch from vacuum to controlled atmosphere; E lab-made compact "control box"; F lab-made color screen data display.

3.4 Assessment of the calcination yield

The experimental device makes it possible to measure the quantity of CO_2 produced by calcination and also to evaluate the shape and appearance of the areas impacted by the interaction between the laser and the sample. The CO_2 sensor used is designed to operate around atmospheric pressure. A specific protocol is therefore

applied. For each sample tested, the chamber and the main optical window are first cleaned. The sample is then placed in the chamber under primary vacuum; the height is adjusted so that the focal plane of the focusing lens is positioned on the surface of the sample. The chamber is then isolated from the pump and an air inlet allows the pressure to rise to atmospheric pressure. The air or gas inlet valve is then closed. The information from the sensors is then read after a stabilization time of 5 min (imposed by the infrared CO₂ sensor). The laser exposure is then carried out at desired intensity and duration. The CO₂ is monitored 5 minutes after laser exposition, permitting quantification of the CO₂ released by the increase in CO₂ above ambient atmospheric concentration. The protocol is repeated for the next measurement with, if necessary, a displacement of the sample using the XY movement platform. Observations of the Heat Affected Zone (HAZ) are carried out outside the sample chamber using a binocular microscope.

3.5 Gas collection for isotopic measurements

Laser calcination for isotopic measurements were all performed at a laser power of 25 W (equivalent to an intensity of 20 kW/cm² on the sample surface). The sample chamber and the sampling tube were first evacuated for 3 minutes. The sampling tube valve was then closed. The laser was then turned on and the sample was rastered until 300 mbar of gas was produced (corresponding to a surface of around 1 cm²). When the desired pressure is obtained (between 1 and 2 minutes), the laser was turned off and the evolved gas transferred to the sample tube by gas pressure equilibration (2 minutes).

3.6 μ XRF

μ XRF elemental mapping of the heat affected zone (HAZ) was performed using a Bruker M4 Tornado μ XRF fast mapping instrument operating under vacuum (20 mbar) at 50kV and 600 μ A with a dwell time of 6 ms/pixel. Data were visualized in relative intensities using the Bruker Tornado software with spectral deconvolution applied.

4. Results

4.1 Calcination threshold

The heat affected zone (HAZ) is a first order means of describing laser-material interaction. This HAZ corresponds to the volume of material where the interaction between the laser light and the irradiated material causes a change in color, volume or density, or even in chemical composition. The area of this zone can be smaller than the laser spot or larger depending on the temperature locally reached in the material. In general, the material transformation effects take place when an intensity threshold is reached. This threshold depends on the ensemble of optical, thermal and mechanical parameters of the irradiated material. The materials considered in this work being very diverse, variable transformation thresholds can be expected. Likewise, they are relatively inhomogeneous in general and it is therefore necessary to repeat each measurement point to obtain a statistical understanding of the probability of transformation. Calcination is primarily assessed based on the appearance of HAZ laser pits after individual laser pulses (Figures 2 and 4). To achieve a representative laser shot, the laser current was adjusted for a 5s pulse, with 1s of rise and fall time on either side; the optical pulse duration due to current threshold for laser emission can be approximated to a constant to 5s.

The probabilities of inducing calcination were measured according to the laser intensity applied on the sample following the method describe in paragraph 3.4. We present below the results for the Death Valley Stromatolite (SDV, sample 8) as it is a homogeneous sample in terms of mineralogy. Figure 2 shows photographs of the HAZ laser pits at the surface and at depth obtained using a laser intensity of 13 kW / cm^2 over 5 s; the white area is lime which crumbles into a very fine white powder after hydration.

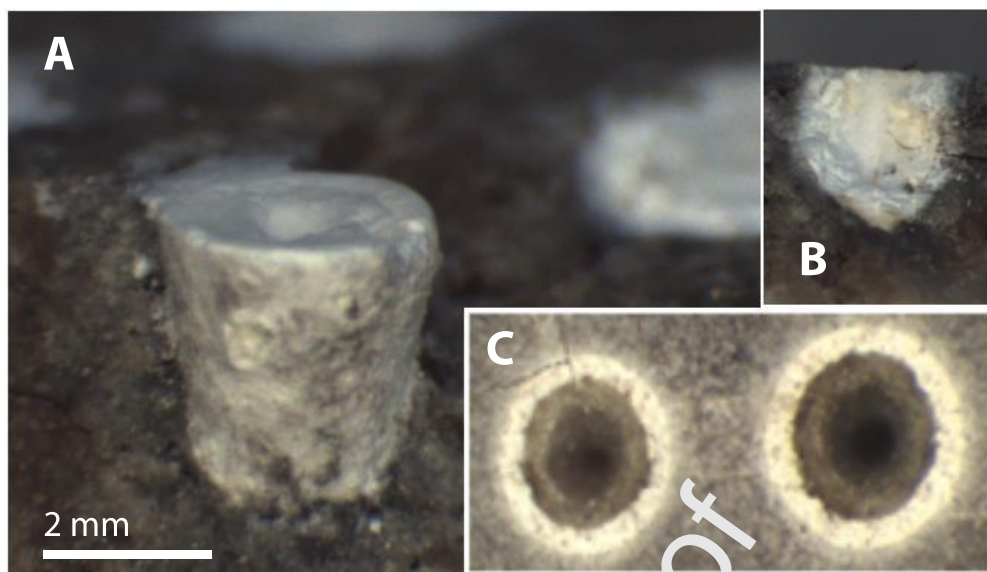


Figure 2: Photography of sample SDV after treatment of 16 W of laser light corresponding to an intensity of 13 kw/cm^2 -5 s. The diameter of HAZ is around 2 mm and depth around 3-4 mm (30 A/5 s). A and B side view, C front view.

Figure 3 shows a μXRF chemical map performed in side view on a HAZ of this sample. Locally increased Ca intensities reveal the presence of CaO, which has a higher volumetric Ca concentration relative to $(\text{Ca-Mg})\text{CO}_3$. It can be seen that CaO production is focused on the crater walls and floor, and does not appear to extend more than a mm from the crater wall into the bulk sample.

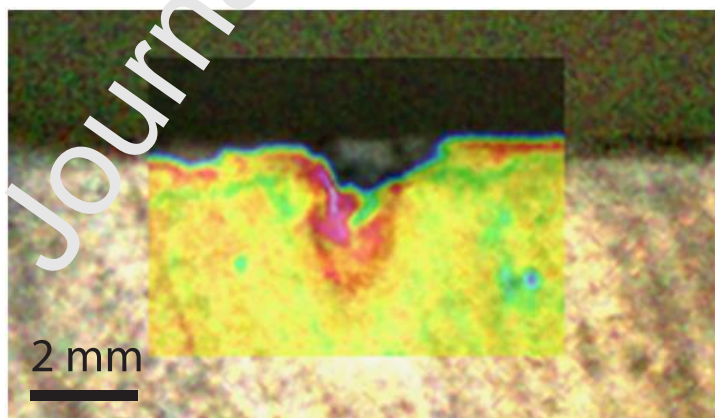


Figure 3: μXRF Ca chemical mapping (relative color scale) in side view of a HAZ of sample SDV after calcination.

Figure 4 shows the histogram of calcination (inferred by the appearance of the HAZ laser pit) as a function of the intensity. The experiment was made 10 times for each intensity and the height of the bar gives the number of events observed at each intensity.

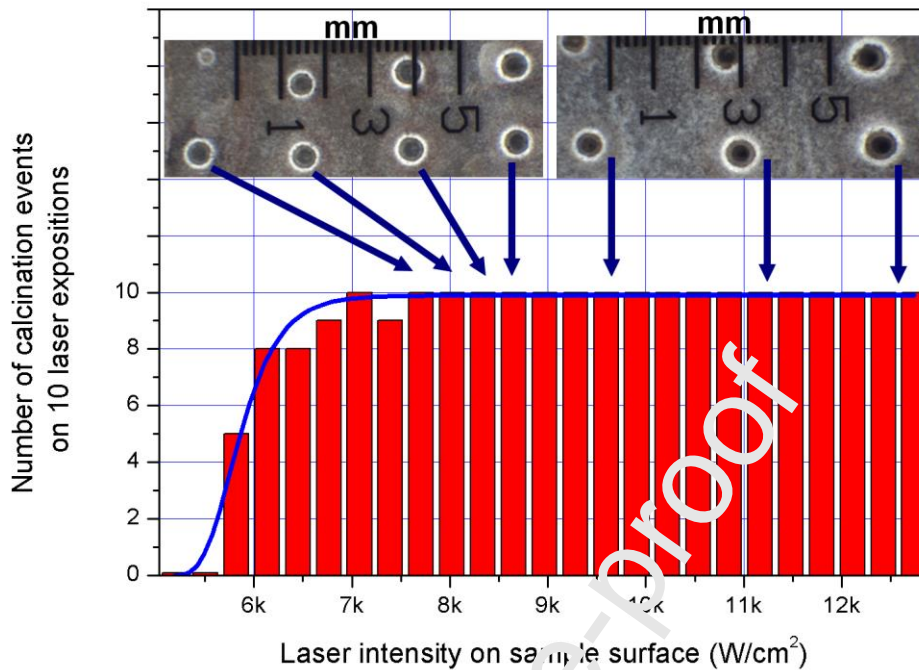


Figure 4: Histogram of calcinations events as a function of laser intensity for the SDV sample at a constant exposure time of 5s.

The transformation threshold for an exposure time of 5 s is thus estimated at around 7-8 kW/cm², and at 9 kW/cm² the probability of observing HAZ laser pits is 100% (notice that the sizes of HAZ laser pits are not evolving with the laser intensity above this threshold, Figure 4). This experiment was repeated for two other samples of different colors and mineral compositions: malachite and aragonite. The transformation thresholds, with an exposure time of 5 s, are 2 kW/cm² and 3 kW/cm² for malachite and aragonite, respectively, showing a strong dependence of the sample characteristics on the calcination threshold. Moreover, **we observe that above the specific threshold of a given type of carbonate the probability of triggering calcinations is 100% and does not depend on impurities, grain boundaries, inclusion or cracks.**

4.2 CO₂ release efficiency

We estimate the amount of CO₂ released for variable parameters of laser intensity and exposure duration in order to verify if CO₂ production is linear as a function of these parameters and to assess thresholds and efficiency for the different studied

materials. For this, we used 2 different samples: malachite and SDV-stromatolite. The measurements are made in ppm and were converted into a mass of CO₂ using the known volume of the chamber (115 cm³). In our experimental setup, 1 ppm corresponds to 2.03 10⁻⁴ mg of CO₂.

Figure 5 shows the mass of CO₂ produced as a function of laser intensity for a constant exposure time of 5 s. The 2 samples show a linear variation in the mass of CO₂ produced by laser calcination (R above 0.99). The thresholds and slopes calculated by linear regression are very different from one sample to another. The thresholds are 2 and 7 kW/cm² and the slopes are 3.3 10⁻⁴ and 0.8 10⁻⁴ mg/(W/cm²) for Malachite and SDV, respectively. These differences are expected with materials whose coefficient of reflection and absorption can strongly vary from one chemical composition to another (Othman et al., 2019). Likewise the thermal properties and enthalpy of calcination will also vary greatly from one chemical composition and structure to another. However, the linear behaviour of CO₂ release as a function of laser intensity is verified in each case.

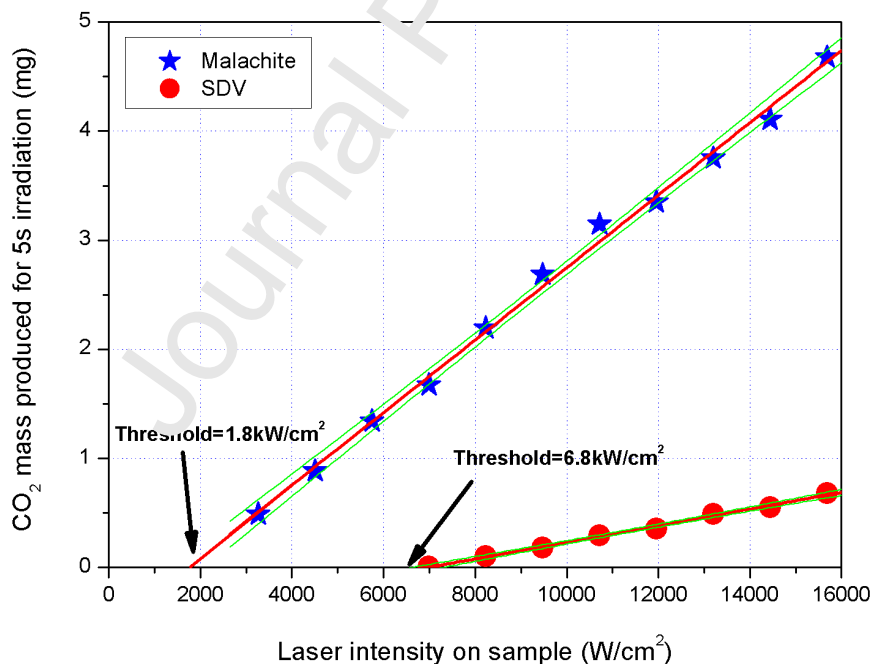


Figure 5: Mass of CO₂ (mg) produced as a function of laser intensity (W/cm²) on the sample for 5 s exposure time for malachite and SDV dolomicrite (red line: linear fit, green lines: 95% confidence intervals)

Further experiments were carried out to determine how the different parameters (laser intensity vs. the duration of exposure) contribute to optimization of the

calcination process. Figure 6 and Figure 7 show two examples of results obtained for two different materials in terms of calcination efficiency. Figure 8 shows the CO_2 released (in ppm) from Malachite as a function of the incident laser energy by comparing two heating modes: a constant exposure time (5 s) with variable intensity vs. a fixed intensity (6 kW/cm^2) with variable exposure time (1 to 10 s in addition to rise and fall times of 1 s each). The incident energy is simply calculated by the product of the incident laser power multiplied by the exposure time. We observe two regression lines ($R^2 = 0.99$) with a difference of a factor of 2 in their slopes (Fig. 8). The two curves intersect close to the typical operating conditions (i.e. $I = 6 \text{ kW/cm}^2$ and $\Delta t = 5 \text{ s}$). These differences demonstrate that it is much more efficient to increase incident laser power than exposure time, and hence that working with high laser intensities over shorter exposure times constitutes the most efficient operating approach. Moreover, it is more difficult to reach the calcination temperature, to maintain it and to provide the necessary energy of enthalpy with a longer exposure time than with a stronger intensity. In the case of long exposure time, thermal losses induced by thermal conductivity and diffusivity are also increased.

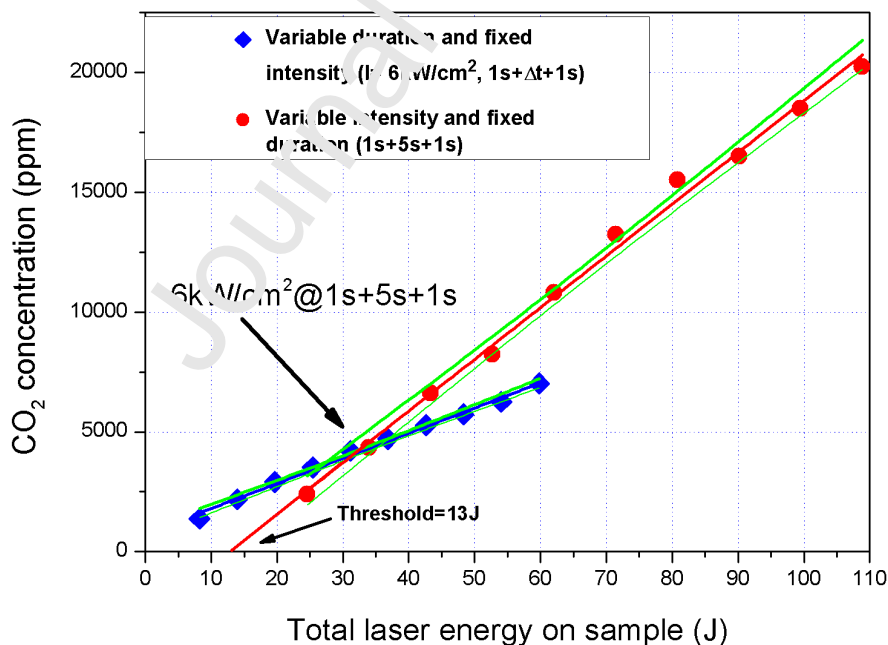


Figure 6: Evaluation with Malachite of the CO_2 concentration as a function of the incident laser energy for two different approaches: at constant exposure time and adjustable intensity and at fixed intensity and variable exposure time (red and blue lines: linear fit, green lines: 95% confidence intervals).

Malachite has a very favourable threshold and slope for CO₂ production. However, this is not a common type of carbonate in comparison to calcite or dolomite, which have more interest as paleoenvironmental archives. Accordingly, the same kind of measurements were applied to the SDV sample, with two different fixed exposure times (5 and 10 s) and variable laser intensity. In Figure 7 the quantity of CO₂ produced is expressed as a function of the incident laser energy. We observe again two regression lines ($R^2 = 0.99$) with similar slopes but very different thresholds. In the case of SDV dolomite, variation in exposure duration does not change the linear relationship between laser energy and CO₂ production (reduction by about 15% between 5 s and 10 s) but the threshold for calcination is more than doubled with an increase of 140%. Moreover, we notice that with the SDV sample the intensity threshold for calcination is very high compared to malachite (see Figure 6). The calcination threshold is therefore much more difficult to reach for dolomite compared to malachite. The laser intensity must all the higher, but similar to the case of malachite, it is again more efficient to favour higher intensity than longer exposure time, the latter being associated with higher thermal losses.

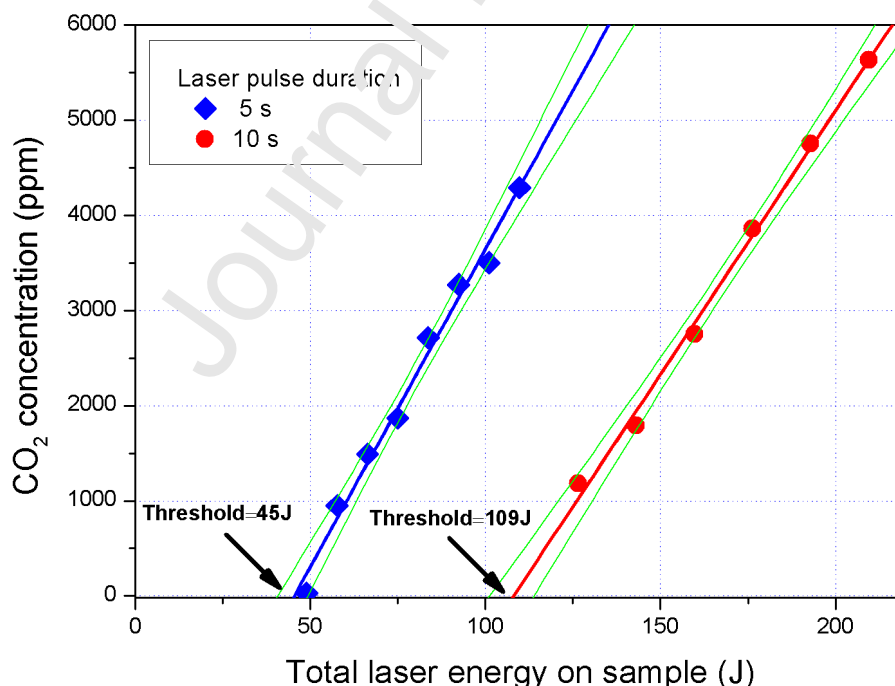


Figure 7: Concentration of CO₂ as a function of incident laser energy with SDV for two exposure times and variable intensity (red and blue lines: linear fit, green lines: 95% confidence interval).

4.3 Isotopic results

All samples were first micro-drilled several times along their surface before being irradiated using the laser system (Figure 8). Isotopic results of both techniques are given in Table 2.

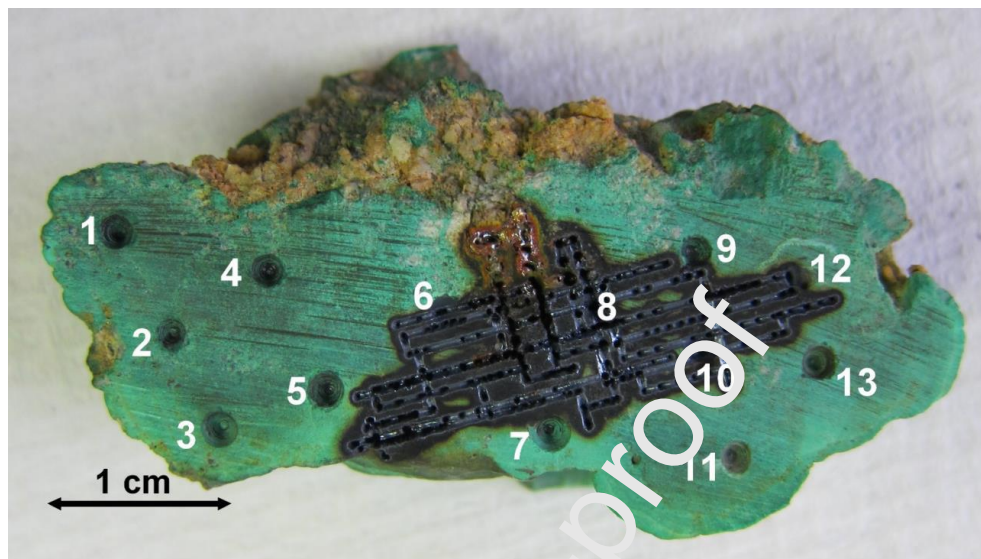


Figure 8: Malachite sample after micro-drilling and laser irradiation

4.3.1 Isotopic sample heterogeneity and analytical reproducibility

Spatial variability in sample isotopic composition as determined by micro-drilling and classic IRMS analysis is quantified in Table 2 by the standard deviation of $\delta^{13}\text{C}$ and $\delta^{18}\text{O}$ and represented graphically for calcite and malachite samples in Figure 9.

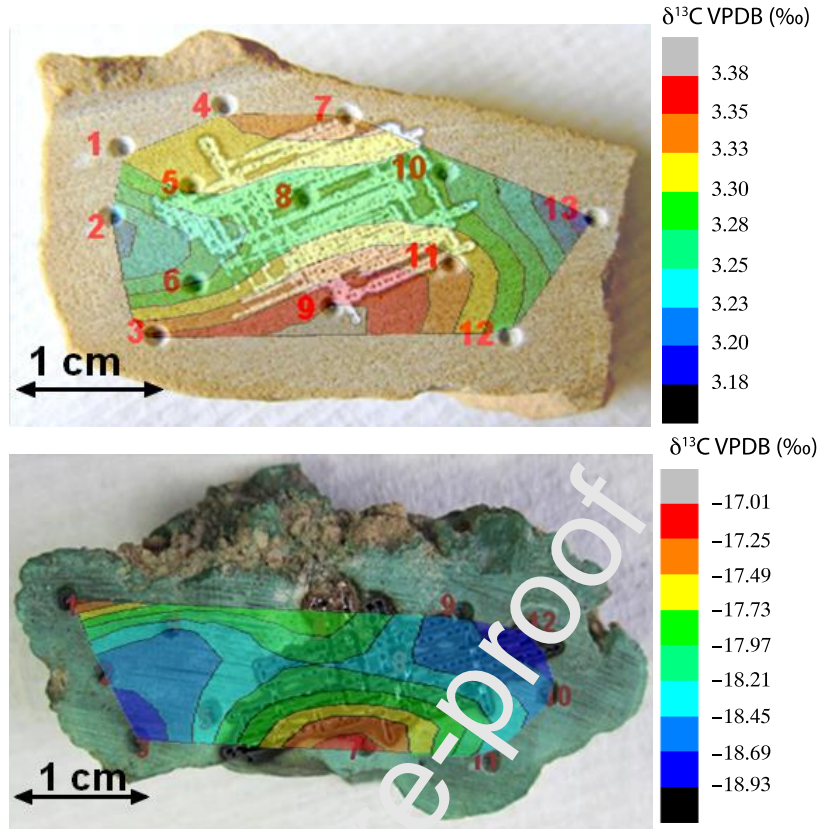


Figure 9: Photographs of sample 2 (SDV Dolomite) and sample 6 (Malachite). Each number represents the microdrill subsample analyzed to estimate the isotopic homogeneity in $\delta^{13}\text{C}$ and $\delta^{18}\text{O}$ of the sample. The white or dark layers correspond to the holes made by the laser as described below. The color map with color scale on the right presents the mathematical fitting of isotopic variations on the sample surface after “microdrill” analyses.

	Classical technique					Laser calcination								
	Number of microdrilling analyses	$\delta^{13}\text{C}$ ‰ VPDB	Standard deviation (1 σ)	$\delta^{18}\text{O}$ ‰ VPDB	Standard deviation (1 σ)	Number of laser calcination repeats	$\delta^{13}\text{C}$ ‰ VPDB	Standard deviation (1 σ)	$\delta^{18}\text{O}$ ‰ VPDB	Standard deviation (1 σ)	m/z 44 (mV) CO ₂	m/z 40 (mV) Ar	m/z 28 (mV) N ₂	m/z 32 (mV) O ₂
Calcite 1	6	4.90	0.66	-3.55	0.39	1	3.96		-13.73		2221	32	2242	573
Calcite 2	7	-0.64	1.33	-14.29	0.57	1	-1.51		-22.59		ND	ND	ND	ND
Dolomite 1	9	2.31	0.16	-6.01	0.18	1	1.78		-15.50		2042	38	2303	527
Dolomite 2	13	3.30	0.05	-1.74	0.16	2	2.62	0.61	-12.34	1.19	2867	28	1877	416
Sidérit	9	-12.22	0.14	-14.57	0.27	2	-	0.21	-22.29	0.20	2642	26	1778	284

e							11.38							
Malachite	13	-18.24	0.66	-3.30	0.23	3	-18.00	0.27	-13.76	1.40	2683	27	1563	463
Rhodocrosite	16	-12.33	0.52	-4.53	0.17	1	-12.27		-9.64		1878	115	6089	1348
SDV	5	-3.01	0.07	-6.05	0.10	5	-2.53	0.17	-14.92	0.19	ND	ND	ND	ND

Table 2: Stable isotope compositions of carbon and oxygen measured after classical “acid technique” and laser CO₂ released experiments performed on 1cm² of samples and gas relative concentration of samples collected after laser calcination. ND: non-determined.

Overall, the standard deviations of repeated analyses of samples after micro-drilling are in most cases below 1‰ for both the $\delta^{13}\text{C}$ and $\delta^{18}\text{O}$ values. Some samples (e.g. Dolomite 1, see table 2) are highly homogeneous with standard deviation within uncertainties of the measurements, while the calcite 2 sample shows resolvable inhomogeneity with standard deviations of 1.33 and 0.57 for the $\delta^{13}\text{C}$ and $\delta^{18}\text{O}$ values, respectively. The standard deviations of repeated laser calcination rastering analyses are larger than those obtained by micro-drilling for both $\delta^{13}\text{C}$ and $\delta^{18}\text{O}$, except for the $\delta^{13}\text{C}$ of the malachite sample (3 rastering repeats) and the $\delta^{18}\text{O}$ of the siderite sample (2 rastering repeats). Finally, we observe a significantly higher standard deviation for the malachite sample $\delta^{18}\text{O}$ (i.e. 1.40‰) after repeated laser calcination, which we hypothesize to arise from the fact that malachite is a copper carbonate hydroxide mineral ($\text{Cu}_2\text{CO}_3(\text{OH})_2$), containing additional oxygen atoms compared to the other samples of this study and whose contribution to the isotope signal during laser calcination is unknown.

4.3.2 Carbon isotope inter-calibration

Figure 10 reports the $\delta^{13}\text{C}$ values measured using the state-of-the-art acid technique versus the new laser protocol.

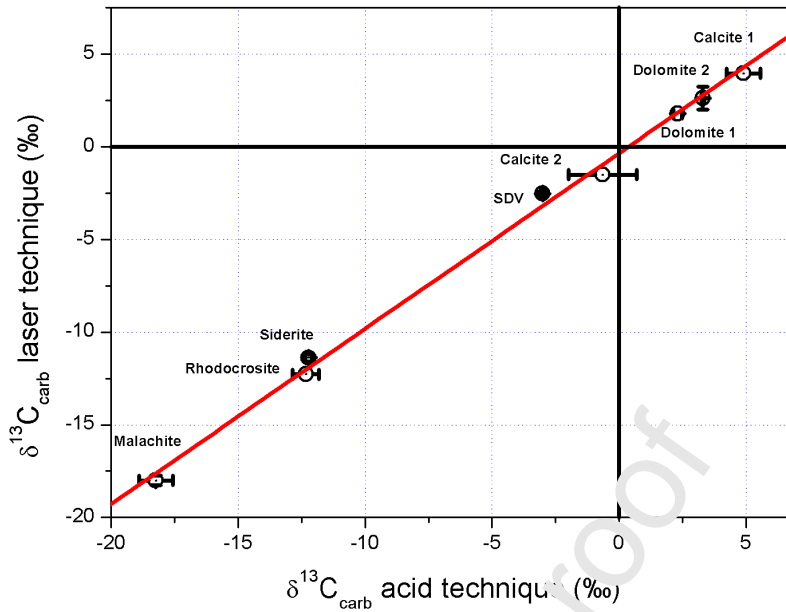


Figure 10: Carbon isotope results for carbonates after laser and acid treatments in ‰ VPDB.

Carbon isotope values determined by both techniques compared very well, with a correlation coefficient of 0.996 and a slope of 0.95. The intercept of the linear regression is close to the origin, with an offset of -0.35‰ , which falls in the range of sample $\delta^{13}\text{C}$ inhomogeneity described in paragraph 4.3.1 (see also Table 2). Moreover, no systematic offset is observed between both techniques (Table 3) and the absolute difference is very close to zero with a mean value of $-0.17 \pm 0.67\text{‰}$ (1σ).

isotopic differences between laser and classical technique (laser - acid)						
	$\delta^{13}\text{C}$ ‰ VPDB	Mean	Standard deviation (1σ)	$\delta^{18}\text{O}$ ‰ VPDB	Mean	Standard deviation (1σ)
Calcite 1	-0.94	-0.17	0.67	10.18	9.38	1.12
Calcite 2	-0.87			8.30		
Dolomite 1	-0.53			9.49		
Dolomite 2	-0.68			10.60		
Sid�rite	0.84			7.72		
Malachite	0.24			10.46		
Rhodocrosite	0.06					
SDV	0.48			8.88		

Table 3: Measured isotopic differences between laser and classical techniques used in this study to measured carbon and oxygen isotopes of carbonates.

Overall, the intercalibrations demonstrate the robustness of the laser calcination method, without any noticeable effect related to the mineralogy of the samples over a large range of isotopic compositions (between around -18 to 5‰), encompassing most of the variability of Earth's natural carbonates.

4.3.3 Oxygen isotopes inter-calibration

Figure 11 reports the $\delta^{18}\text{O}$ values measured using the state-of-the-art acid technique versus the new laser protocol. Notice here that the $\delta^{18}\text{O}$ value of Rhodochrosite is excluded from this comparison due to strong O_2 -bearing air contamination (see Table 2).

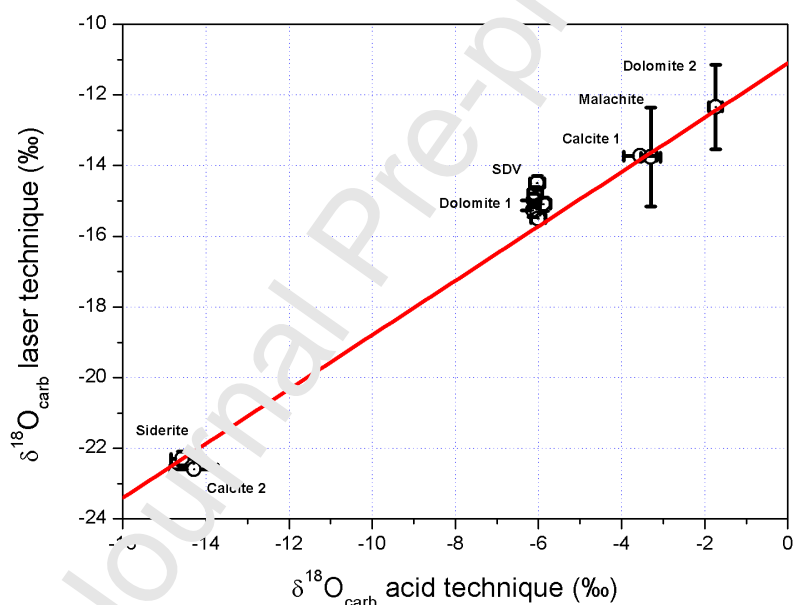


Figure 11: Oxygen isotopes results of carbonates (Rhodochrosite excluded) after laser and acid treatments in ‰ VPDB.

Both techniques compared well, with a correlation coefficient of 0.986 over a large range of isotopic compositions (spanning ca. -15 to -2‰). However, the slope of the linear regression fit is significantly different from 1 with a value of 0.77. The intercept is also significantly deviated from the origin with an intercept at -10.88‰, the laser data being systematically enriched in ^{16}O . This systematic difference is also illustrated in Table 3 with an absolute difference between both techniques (i.e. laser – acid) of $9.38 \pm 1.12\text{‰}$ (1σ).

Therefore, the intercalibration is also favorable for oxygen isotopes, over a large range of carbonate lattice configurations and isotopic compositions. However, a correction factor, reflecting a laser calcination isotopic equilibrium or pseudo-equilibrium between CaO and CO₂, has to be applied to report the results on the VPDP scale. This isotopic effect has yet to be characterized in detail and should be considered in more detail in future studies in order to verify if a single correction factor can be applied on serial analyses of samples.

5. Discussion

The new fiber coupled laser diode technique described here compares well in performance with previous laser-based methods for carbonate isotope analyses (Smalley et al., 1989; Smalley et al., 1992; Sharp, 1992; Sharp and Cerling, 1996; Cerling and Sharp, 1996; Spötl and Matthey, 2006). Table 4 summarises the results of this study and six previous published techniques, based on either Nd:YAG or CO₂ lasers, in terms of spot size, gas purification steps, analysis time, reproducibility, and apparent isotopic shifts between laser ablation and conventional acid digestion analysis. The fiber coupled laser diode technique examined in this study shows a 1-standard-deviation reproducibility that is effectively equivalent to that obtained by prior published laser ablation techniques for $\delta^{13}\text{C}$ (0.3‰ vs. 0.2 to 0.5‰ in previous studies), and only slightly greater relative to prior techniques for $\delta^{18}\text{O}$ (0.7‰ vs. 0.1 to 0.5‰ in previous studies). For $\delta^{13}\text{C}$ determination, the fiber coupled laser diode method shows excellent agreement with results obtained by conventional acid digestion analyses. However, in the case of $\delta^{18}\text{O}$, we observed a strong isotopic shift ($-9.4\text{‰} \pm 1.1$) relative to values obtained by conventional acid digestion analyses, which was relatively constant across the different replicates and minerals examined, permitting the application of a constant correction factor for the conditions examined herein. Such an important degree of fractionation of oxygen isotopes during laser ablation has been observed previously and attributed to the fact that only 2/3 of the oxygen atoms are removed from the carbonate during laser heating (equation (1)) (Sharma and Clayton, 1965). However, we notice that compared to previously published techniques (Figure 4), the partitioning seems to be constant throughout our set of samples, but that the value of this offset is higher than previously observed. This shift warrants further examination in future work; additional experiments may

resolve whether it represents a kinetic isotope or partial reaction effect, in which case the shift might be modified under different laser ablation conditions such as the intensity delivered at the focal point or duration (see supplementary information for a laser type comparison), or whether it represents an equilibrium fractionation between CO₂ and CaO (and/or other relevant species) that would remain largely constant if equilibrium conditions were consistently achieved. Mass scans revealed no significant amount of carbon monoxide (data not shown), which had previously been suggested as a possible issue for laser pulses of ≥ 1 s duration (Powell and Kyser, 1991). The ratio of ions at m/z 28 and 32, reflecting the O₂ / N₂ ratios of analysed sample gases (Table 2), were very close to the atmospheric ratio of 4, pointing to trace air in the system rather than any significant CO production.

	Smalley et al., 1989	Smalley et al., 1992	Sharp, 1992	Sharp and Cerling, 1996	Cerling and Sharp, 1996	Spötl and Matthey, 2006	This study
Laser type	Nd:YAG	Nd:YAG	CO ₂	CO ₂	CO ₂	CO ₂	Laser diode
minimum spot size	10 μ m	25 μ m	80 μ m	100 to 200 μ m	200 to 250 μ m	300 μ m	400 μ m
Gas purification steps	cold trap	cold trap	cold trap	continuous flow He-GC	cold trap and continuous flow He-GC	continuous flow He-GC	direct gas injection in mass spec
Total time of one analysis	nd	30 minutes	nd	nd	nd	3 minutes	few minutes

Isotopic differences between laser and conventional acid digestion	1.7 (calcite) to 2.5 (aragonite) ‰ for $\delta^{18}\text{O}$; no correction for $\delta^{13}\text{C}$	1.2‰ for $\delta^{18}\text{O}$; -0.8‰ for $\delta^{13}\text{C}$	nd	0.3 (calcite) to 2.1 (siderite) ‰ for $\delta^{18}\text{O}$; 0.05±0.3 ‰ for $\delta^{13}\text{C}$ (excluding siderite at ca. 2‰)	0.68±0.67 ‰ for $\delta^{13}\text{C}$ (oxygen isotopes are a mixture of CO_3 and PO_4 in this case)	-1.14‰ for $\delta^{18}\text{O}$; 0.14‰ for $\delta^{13}\text{C}$	-9.38 ±1.12‰ for $\delta^{18}\text{O}$; -0.17 ±0.67‰ for $\delta^{13}\text{C}$
Reproducibility of replicate laser analyses (1σ)	±0.2‰ for $\delta^{18}\text{O}$ and $\delta^{13}\text{C}$	±0.4‰ for $\delta^{18}\text{O}$; ±0.2‰ for $\delta^{13}\text{C}$	±0.1‰ for $\delta^{18}\text{O}$; ±0.2‰ for $\delta^{13}\text{C}$	±0.29‰ for $\delta^{18}\text{O}$; ±0.19‰ for $\delta^{13}\text{C}$	±0.3‰ for $\delta^{18}\text{O}$ and ±0.2‰ for $\delta^{13}\text{C}$	±0.3‰ for $\delta^{18}\text{O}$ and ±0.2‰ for $\delta^{13}\text{C}$	±0.7‰ for $\delta^{18}\text{O}$ and ±0.3‰ for $\delta^{13}\text{C}$
Type of carbonates analyzed	calcite and aragonite	calcite and dolomite	metamorphic calcite and dolomite	calcite, dolomite, magnesite, rhodocrosite, siderite and smithsonite	Tooth enamel	Carrara marble	calcite, dolomite, malachite, rhodocrosite, siderite

Table 4: Comparison of different laser analytical methods applied to carbonate stable isotope analyses.

While the analytical performance of the fiber coupled diode laser calcination system is comparable to previous systems, it has several additional advantages over previous systems. First, the system examined in this study appeared to be largely immune to matrix effects, at the cm^2 scale of analysis presented here, providing robust results for a wide range of carbonate minerals. Additionally, no gas purification steps nor consumable reagents were required, which opens the door to systems of significantly reduced complexity. Furthermore, fiber coupled diode lasers are readily available, highly compact, affordable, and highly adjustable in terms of laser intensity and shot duration. This combination of characteristics provides for a highly compact laser ablation system (benchtop for the current setup), and more importantly, may enable novel applications in the future. For example, such a system could easily be made portable, deployable on-site or in the field, where samples could be prepared as glass vials containing CO_2 gas ready for later offline IRMS analyses after laser calcination of centimetric surfaces. Even more exciting is the potential of coupling

such a system to a sufficiently compact spectroscopy-based CO₂ isotope ratio analyzer (e.g., CRDS or IRIS) such that a single highly compact (e.g., automobile-portable) system would be capable of producing high-quality spatially-resolved C and O isotope compositions of carbonate minerals directly in the field, or integrated as an additional analytical component in multi-parameter core scanner device. Future developments also include the possibility of down-scaling isotopic measurements in the micro-metric range of analysis (i.e. single laser pulses) after careful examinations of possible micro-scale isotopic effects due to impurities, inclusions or variations in crystal lattice.

6. Conclusions

We report that the use of the coupled diode laser calcination system for analyzing the stable carbon and oxygen isotopic composition of carbonates gives reproducible results that can be scaled to the state of the art acid dissolution technique without correction for $\delta^{13}\text{C}$ and after calibration for $\delta^{18}\text{O}$. Moreover, intercalibration results demonstrate that this new laser calcination method, at the centimeter scale, compares well with classical methods for carbonates of different mineralogies and over a large range of isotopic compositions for both carbon and oxygen isotopes.

This new calcination method using a fiber coupled laser diode for the stable isotope analysis of carbonate has several important advantages over previous methods. Compared to acid dissolution techniques, this method drastically reduces the time of analysis while also offering spatially resolved isotopic characterization. While previous automated CO₂ laser ablation techniques have been proven to efficiently perform high resolution $\delta^{18}\text{O}$ and $\delta^{13}\text{C}$ measurements of laminated speleothems (Spötl and Matthey, 2006; McDermott, 2005; Cosford et al., 2008; Hodge et al., 2008; Cosford et al., 2009; Cosford et al., 2010; Baker et al., 2011; Baldini et al., 2015), the system presented here extends the range of possible analyses to other type of carbonate samples using a single fiber coupled laser diode-induced calcination module. Furthermore, fiber coupled diode lasers are highly compact compared to previous laser systems and can be paired with field-deployable CRDS/IRIS optical-mass spectrometers, opening the door to novel on-site or in the field applications in the near future.

Acknowledgements

This work is a contribution to the “Investissements SATT SAYENS” project ISOLASER and was also supported by the Observatoire des Sciences de l’Univers Terre Homme Environnement Temps Astronomie de Franche-Comté-Bourgogne (OSU THETA), and by the FEDER Bourgogne Franche-Comté. The authors would like to thank SATT Ovest for their assistance with this project. The authors also would like to apologise to the LGO ICP-MS laboratory for having exploded a laser ablation cell and to the IPGP stable isotope laboratory for inducing temporary blindness during early tests. We also thank Céline Liorzou for her assistance with early tests. Jerome Thomas is warmly acknowledged for providing access to the Dijon Museum collection of minerals. Sofiane Lazali is acknowledged for his initial work on sorting and micro-drilling the samples of his study. Baptiste Paulmier is acknowledged for his work on the electronic parts of the system. We thank Craig Smalley and an anonymous referee for their constructive reviews and Michael E. Böttcher for handling this contribution.

References:

Berner, R. A., Lasaga, A. C., & Garrels, R. M. (1983). The carbonate-silicate geochemical cycle and its effect on atmospheric carbon dioxide over the past 100 million years. *AmJS*, 283(7), 641-683.

Walker, J. C., Hays, P. B., & Kasting, J. F. (1981). A negative feedback mechanism for the long-term stabilization of Earth's surface temperature. *Journal of Geophysical Research : Oceans*, 86(C10), 9776-9782.

McCrea, J. M. (1950). On the isotopic chemistry of carbonates and a paleotemperature scale. *The Journal of Chemical Physics*, 18(6), 849-857.

Garcia-Anton, E., Cuezva, S., Fernandez-Cortes, A., Benavente, D., & Sanchez-Moral, S. (2014). Main drivers of diffusive and advective processes of CO₂-gas exchange between a shallow vadose zone and the atmosphere. *International Journal of Greenhouse Gas Control*, 21, 113-129.

Rizzo, A. L., Jost, H. J., Caracausi, A., Paonita, A., Liotta, M., & Martelli, M. (2014). Real-time measurements of the concentration and isotope composition of atmospheric and volcanic CO₂ at Mount Etna (Italy). *Geophysical Research Letters*, 41(7), 2382-2389.

Fischer, T. P., & Lopez, T. M. (2016). First airborne samples of a volcanic plume for $\delta^{13}\text{C}$ of CO_2 determinations. *Geophysical Research Letters*, *43*(7), 3272-3279.

Smalley, P. C., Stijfhoorn, D. E., Råheim, A., Johansen, H., & Dickson, J. A. D. (1989). The laser microprobe and its application to the study of C and O isotopes in calcite and aragonite. *Sedimentary Geology*, *65*(3-4), 211-221.

Smalley, P. C., Maile, C. N., Coleman, M. L., & Rouse, J. E. (1992). LASSIE (laser ablation sampler for stable isotope extraction) applied to carbonate minerals. *Chemical Geology: Isotope Geoscience section*, *101*(1-2), 43-52.

Sharp, Z. D. (1992). In situ laser microprobe techniques for stable isotope analysis. *Chemical Geology: Isotope Geoscience section*, *101*(1-2), 3-19.

Sharp, Z. D., & Cerling, T. E. (1996). A laser GC-IRMS technique for in situ stable isotope analyses of carbonates and phosphates. *Geochimica et Cosmochimica Acta*, *60*(15), 2909-2916.

Cerling, T. E., & Sharp, Z. D. (1995). Stable carbon and oxygen isotope analysis of fossil tooth enamel using laser ablation. *Palaeogeography, Palaeoclimatology, Palaeoecology*, *126*(1-2), 173-186.

Spötl, C., & Matthey, D. (2006). Stable isotope microsampling of speleothems for palaeoenvironmental studies: a comparison of microdrill, micromill and laser ablation techniques. *Chemical Geology*, *235*(1-2), 48-58.

McDermott, F. (2005). Centennial-scale Holocene climate variability revealed by a high-resolution speleothem $\delta\text{O}-18$ record from SW Ireland. *Science*, *309*, 1816-1816.

Cosford, J., Qing, H., Eglington, B., Matthey, D., Yuan, D., Zhang, M. & Cheng, H. (2008) East Asian monsoon variability since the Mid-Holocene recorded in a high-resolution, absolute-dated aragonite speleothem from eastern China. *Earth and Planetary Science Letters*, *275*, 296-307.

Hodge, E. J., Richards, D. A., Smart, P. L., Andreo, B., Hoffmann, D. L., Matthey, D. P. & Gonzalez-Ramsan, A. (2008) Effective precipitation in southern Spain (266 to 46ka) based on a speleothem stable carbon isotope record. *Quaternary Research*, *69*, 447-457.

Cosford, J., Qing, H., Matthey, D., Eglington, B. & Zhang, M. (2009) Climatic and local effects on stalagmite $\delta^{13}\text{C}$ values at Lianhua Cave, China. *Palaeogeography, Palaeoclimatology, Palaeoecology*, *280*, 235-244.

Cosford, J., Qing, H., Lin, Y., Eglinton, B., Matthey, D., Chen, Y.G., Zhang, M. and Cheng, H. (2010) The East Asian monsoon during MIS 2 expressed in a speleothem $\delta^{18}\text{O}$ record from Jintanwan Cave, Hunan, China. *Quaternary Research*, 73, 541-549.

Baker, A., Wilson, R., Fairchild, I. J., Franke, J., Spötl, C., Matthey, D., Trouet, V. & Fuller, L. (2011) High resolution $\delta^{18}\text{O}$ and $\delta^{13}\text{C}$ records from an annually laminated Scottish stalagmite and relationship with last millennium climate. *Global and Planetary Change*, 79, 303-311.

Baldini, L. M., McDermott, F., Baldini, J. U. L., Arias, P., Cueto, M., Fairchild, I. J., Hoffmann, D. L., Matthey, D. P., Müller, W., Nita, D. C., Ontañón, R., García-Moncó, C. & Richards, D. A. (2015) Regional temperature, atmospheric circulation, and sea-ice variability within the Younger Dryas Event constrained using a speleothem from northern Iberia. *Earth and Planetary Science Letters*, 419, 101-110.

Othman, H., San Roman Alerigi, D., Batarseh, S., & Al Obaid, O. (2019, November). Efficiency of High Power Laser in Carbonate Formations. In *Abu Dhabi International Petroleum Exhibition & Conference*. Society of Petroleum Engineers.

Turchetta, S., & Carrino, L. (2005). An energy based model for laser cutting natural stone. *International Journal of Machine Tools and Manufacture*, 45(7-8), 761-767.

San-Roman-Alerigi, D. P., Han, Y., & Batarseh, S. I. (2017). Thermal and geomechanical dynamics of high power electromagnetic heating of rocks. In *SPE Middle East Oil & Gas Show and Conference*. Society of Petroleum Engineers.

San-Roman-Alerigi, D. P., van Dijk, C. P., Lube, V., & Lubineau, G. (2018). Characterizing the Effects of High Power Laser Performance on Carbonate Rocks. *Mineralogy and Geomechanical Analysis for Hydraulic Fracturing: An Integrated Approach to Assess Rock Fracability in Sandstone Reservoirs see page 2 A Field Case Study of an Interwell Gas Tracer Test for Gas EOR Monitoring see page 27*, 47.

Engler, P., Santana, M. W., Mittleman, M. L., & Balazs, D. (1989). Non-isothermal, in situ XRD analysis of dolomite decomposition. *Thermochimica Acta*, 140, 67-76.

Coplen, T. B., Brand, W. A., Gehre, M., Gröning, M., Meijer, H. A., Toman, B., & Verkouteren, R. M. (2006). New guidelines for $\delta^{13}\text{C}$ measurements. *Analytical Chemistry*, 78(7), 2439-2441.

Böttcher, M. E. (1996). $^{18}\text{O}/^{16}\text{O}$ and $^{13}\text{C}/^{12}\text{C}$ fractionation during the reaction of carbonates with phosphoric acid: effects of cationic substitution and reaction temperature. *Isotopes in environmental and health studies*, 32(2-3), 299-305.

Rosenbaum, J., & Sheppard, S. M. F. (1986). An isotopic study of siderites, dolomites and ankerites at high temperatures. *Geochimica et cosmochimica acta*, 50(6), 1147-1150.

Sharma, T., & Clayton, R. N. (1965). Measurement of $\text{O}^{18}\text{O}^{16}$ ratios of total oxygen of carbonates. *Geochimica et Cosmochimica Acta*, 29(12), 1347-1353.

Powell, M. D., & Kyser, T. K. (1991). Analysis of $\delta^{13}\text{C}$ and $\delta^{18}\text{O}$ in calcite, dolomite, rhodochrosite and siderite using a laser extraction system. *Chemical Geology*, 94(1), 55-66.

Journal Pre-proof

Declaration of interests

The authors declare that they have no known competing financial interests or personal relationships that could have appeared to influence the work reported in this paper.

The authors declare the following financial interests/personal relationships which may be considered as potential competing interests:

Journal Pre-proof